second and third rotors. At the end of the transition, when $\gamma(T) = \gamma_0$, we have to stabilize the satellite in the new attitude so that Eq. (14a) is satisfied and, of course, at the end of transition we must have $\dot{\gamma}(T) = 0$.

References

[1] Anchev, A. A., "Flywheel Stabilization of Relative Equilibrium Satellite," *Kosmicheskie Issledovenia,* Vol. 4, 1966, pp. 192–202.

[2] Roberson, R. E. and W. W. Hooker, "Gravitational Equilibria of a Rigid Body Containing Symmetric Rotors," *Proceedings of the 17th Congress of the International Astronautical Federation,* Dunod, Paris, 1967.

[3] Rumiantsev, V. V., *On the Stability of Stationary Motions of Satellites,* Computing Center of Academy of Sciences, USSR press, Moscow, 1967.

[4] Longman, R. W., "A Generalized Approach to Gravity-Gradient Stabilization of Gyrostat Satellites," RM-5921-PR, 1969, The RAND Corp.

[5] Roberson, R. E., "Stability of Orbiting Gyrostats in the Elementary Cases," *Ingenieur-Archiv,* Band 39, Heft 5, 1970, pp. 317–329.

APRIL 1973 AIAA JOURNAL VOL. 11, NO. 4

Experimental and Theoretical Investigation of Stress Wave Attenuation by Inclusions

J. C. S. YANG* AND C. Y. TSUI†
University of Maryland, College Park, Md.

The propagation of an initially sharp cylindrical pressure pulse through a linear elastic medium with inclusions is analyzed, both experimentally and analytically. In the experiment, tests were performed on plates with single and multiple circular inclusions embedded in a matrix of lower characteristic impedance. Sharp compression pulses were generated at an edge of the plate by two methods; the detonation of a charge of lead azide and the impingement of a sharp knife-edged ram impacted at the opposite end by a short projectile. Strain gages were mounted on various positions of the plate to determine the attenuation of the transient stress. The qualitative analytical treatment is based on the methods of propagating stress discontinuities. Computer programs were written to numerically determine the changes in the shape of the leading wave front and the stresses immediately behind it. Experimental results for the attenuation of stress wave on steel-aluminum and steel-brass inclusion-matrix composites compared very well with the computed analytical results.

Introduction

GROWING requirements for lightweight materials with great strength and stiffness, especially in the aerospace field on such projects as STOL, VTOL aircraft, Space Shuttle vehicles, heat shield, etc., have led to increased interest and research in the area of fiber composite materials.

One of the most interesting properties of fiber-reinforced composites is their dispersive characteristics. In general, when a stress pulse is applied to the boundary of a composite, the shape of the pulse is changed, and it "smears out" as it propagates through the slab, with an attenuation of amplitude. Thus the composite appears to have greater dynamic than static strength. However, for dynamic loads, the simplest geometrical configuration may give rise to tensile stresses, even though the loading is compressive. The load-carrying capacity of a body fabricated on a fiber-reinforced composite is adversely affected by bond failure at the interface bonds; in particular, it may be substantially smaller than the strengths of the materials constituting the composite, and relatively small tensile stresses may thus produce bond failure. In addition, fracture and spallation could occur due to the reflection at the back free surface of the slab, and internal stress concentration could occur due to refractions, reflections, and a focusing effect of the geometrical configuration. Few analytical and experimental investigations of such situations appear to have been carried out. In many cases, it is believed that the development of composites has proceeded with little appreciation for the importance of microstructural variables such as interface strength, modulus ratios, fiber size, etc., on the composite strength under stress-wave loading. Consequently, in order to have increased resistance to stress-wave fracture, a better understanding of the micromechanics of the fracture process must be developed. This approach is necessary to guide composite material development, and should result in large-scale practical benefits.

In this paper, we are concerned with the propagation of an initially sharp cylindrical pressure pulse through a linear elastic medium with inclusions. The pattern of transient waves is extremely complicated, and for the analytical treatment, the attention is, therefore, focused on the changes in the shape of the leading wave front and the stress immediately behind it.

The basis for the present approach is the ray tracing and associated wave front analysis of geometrical optics. It can be shown that even in the case of elastic waves with two basic wave speeds in each material, the stress amplitude at the initial

---

Presented as Paper 72-394 at the AIAA/ASME/SAE 13th Structures, Structural Dynamics, and Materials Conference, San Antonio, Texas, April 10–12, 1972; submitted April 25, 1972; revision received September 22, 1972. This work was jointly supported by NASA Ames Research Center under contract NGR-21-002-350; the Minta Martin Fund, College of Engineering and the Computer Science Center, University of Maryland.

Index categories: Structural Dynamic Analysis; Structural Composite Materials (Including Coatings).

* Professor. Member AIAA.

† Assistant Professor.

Fig. 1 Single inclusion specimen.

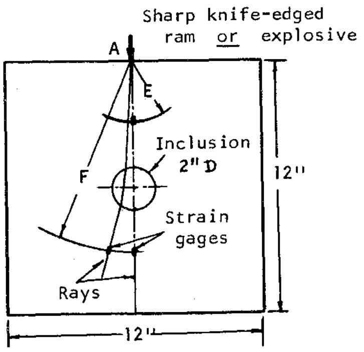

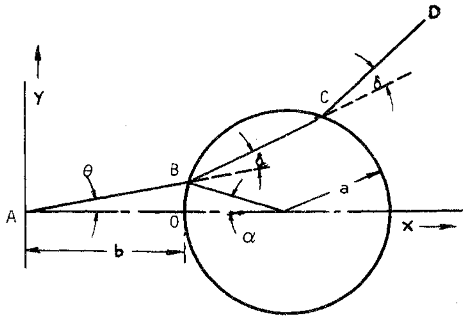

Fig. 3 Geometrical parameters for computation of the wave front.

wave front is given exactly by the law of geometrical optics associated with the propagation of irrotational waves. This follows from application of the theory of characteristics and is in accordance with the more common interpretation of geometrical optics as an approximation to the solution for oscillatory waves at high frequencies. This approach determines the stress tensor at the wave front, and can be extended also to determine stress gradients there.

The propagation of stress discontinuities was discussed in considerable detail by Thomas.[1] Much of the recent work in this area is patterned after that due to Luneburg,[2] for electromagnetic discontinuities, and Friedlander,[3] for the propagation of discontinuities in acoustic media. Propagation of stress discontinuities in elastic media, including the reflections and refractions of discontinuities at interfaces of different elastic solids, was investigated by Keller.[4] An application of wave-front analysis to the problem of an inclusion embedded in an elastic medium was presented by Ting and Lee.[5] Achenbach, Hemann, and Ziegler[6] presented an interesting experiment in studying separation of the interface of a circular inclusion and the surrounding medium. Nariboli[7] combined the ideas of the theory of singular surfaces with those of ray theory. Recently, Ben-Amoz[8] considered the problem of propagation of actual stress pulses through bounded anisotropic media.

Experiments

The specimen used for the experiment consisted of 12 in.^{2} plates made of aluminum or brass with steel inclusions. The inclusions were shrunk fit in the plate with an interface pressure of approximately 200 psi. The steel-aluminum combination has a characteristic impedance ratio of 2.66 and a propagation velocity ratio of 1.03, and the steel and brass have ratios of 1.27 and 1.39, respectively. Four different kinds of specimens were tested—i.e., one, two, three, and four cylindrical inclusions with the total area kept equal. A drawing of a single-inclusion specimen is shown in Fig. 1. In addition, experiments were also conducted on 12 in. × 12 in., 12 in. × 48 in., and 48 in. × 48 in. aluminum plates without inclusion.

The compressive pulse in the plate was generated by two methods: 1) The detonation of lead azide at the center of the upper edge (The plates were placed in a vertical position and supported by rubber pads at the lower corners.); and 2) The impingement of a knife-edged ram (The specimens were supported freely on rollers with the center of one edge resting against the ram. The other end of the ram was impacted by a projectile released from an air gun.) A schematic diagram of this experimental arrangement is given in Fig. 2.

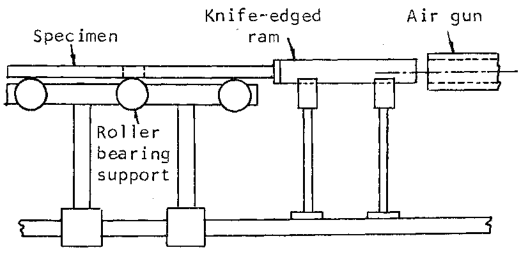

Fig. 2 Experimental arrangement for generation of pulse by impingement of a knife-edged ram.

Both the lead azide charge and the impingement of the sharp ram produced cylindrical waves emanating from the edge at the point of contact into the plate. During the experiment, different amounts of lead azide and several impact velocities and projectile lengths were used. Pairs of strain gages were mounted on the opposite faces of the plate at various positions along the rays (see Fig. 1) to measure the transient stress. Each pair of gages are connected in the opposite arms of a wheatstone bridge circuit to cancel any bending effects. The output signal from the bridge circuit was fed into an oscilloscope.

Analysis

The wave fronts can be located by a direct calculation using Fermat's principle. To illustrate the procedure in computing rays and wave front, let us consider a ray AB in Fig. 3 which strikes the inclusion at angular position θ. For simplicity, distortion wave fronts are omitted and only the rays associated with a compressive wave front are sketched. If a is the radius of the inclusion and b the distance from the applied pressure point to the inclusion, the coordinates of point B are given by $x_B = L_{AB}\cos\theta$ and $y_B = L_{AB}\sin\theta$, where L_{AB} is the length of the straight ray AB and is given by

$$L_{AB} = (b+a)\cos\theta - [(b+a)^2\cos^2\theta - b^2 - 2ab]^{1/2}$$

Let $t = 0$ be the time at which the cylindrical wave initiates at $x = 0$. The time t required for the wave front to reach point B

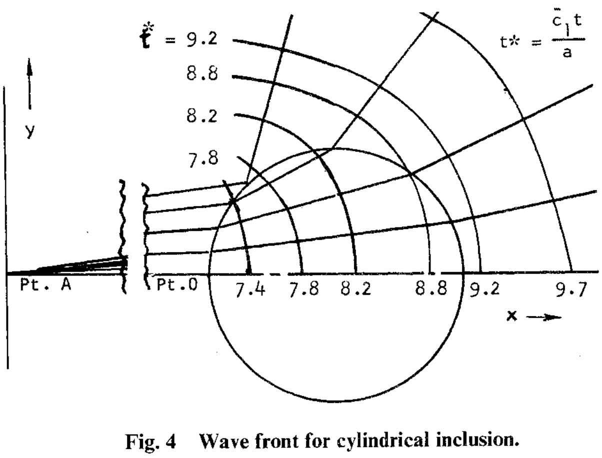

Fig. 4 Wave front for cylindrical inclusion.

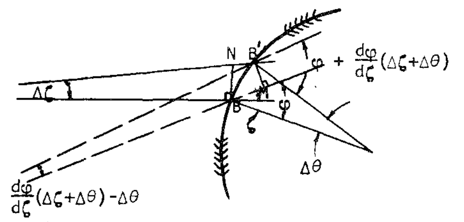

Fig. 5 Refraction of two neighboring rays.

is $t = L_{AB}/c_1$, where c_1 is the speed of longitudinal waves in medium 1. The time t required for point C on the refracted ray BC to be reached by the wave front is

$$t = L_{AB}/c_1 + L_{BC}/c_2, \quad \text{or} \quad L_{BC} = c_2(t - L_{AB}/c_1)$$

where L_{BC} is the length of the straight ray BC and c_2 is the speed of longitudinal waves in medium 2. The inclination of the refracted ray to the incident ray direction, δ, is given by Snell's Law

$$c_1/c_2 = \sin\zeta/\sin\phi \tag{1}$$

where $\zeta = \theta + \alpha$ and $\phi = a + \theta + \delta$.

The coordinates of point C are given by $x_C = x_B + L_{BC}\cos(\theta+\delta)$ and $y_C = y_B + L_{BC}\sin(\theta+\delta)$, where the length L_{BC} can also be expressed by $L_{BC} = 2a\cos\phi$.

A similar calculation determines the wave front after refraction out of the inclusion. The coordinates of point D are given by

$$x_D = x_C + L_{CD}\sin(\theta+2\delta) \quad \text{and} \quad y_D = y_C + L_{CD}\sin(\theta+2\delta)$$

where L_{CD}, the length of the straight ray CD, is determined by

$$t = L_{AB}/c_1 + L_{BC}/c_2 + L_{CD}/c_1 \quad \text{or} \quad L_{CD} = c_1 t - L_{AB} - c_1/c_2\, L_{BC}.$$

The wave fronts as expressed by the aforementioned equations are shown in Fig. 4 for various times.

A complete analytical treatment of the stresses for the wave propagation problem shown in Fig. 1 is very difficult. However, the stresses at the instant that the wave fronts arrive can be obtained in a rather straightforward and simple manner by investigating propagating stress discontinuities. The analysis assumes linear elastic response of the materials of the inclusion and the matrix. In addition, it is assumed that the applied pressure instantaneously rises to a certain value and then rapidly decreases to zero. The stress discontinuity applied on the boundary generates surfaces of discontinuity which propagates into the interior of the continuous body in a manner which was discussed by other authors, most notably by Thomas[1] and Keller.[4] Here we consider the problem in two spatial dimensions. When given the initial signal at a point on each ray, the variation of this signal along the ray is governed by

$$p^2 R = \text{const} \tag{2}$$

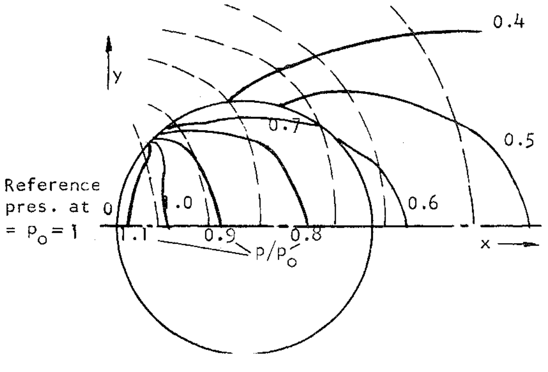

Fig. 6 Pressure at wave front for cylindrical inclusion.

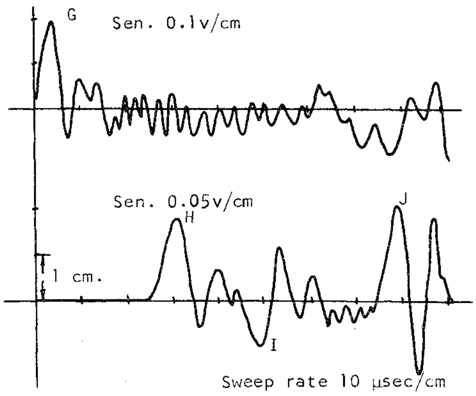

Fig. 7 Reproduction of strain histories due to explosive loading on a single-inclusion steel-aluminum specimen, 0° ray.

Changes in intensity at the boundary between the matrix and inclusions are determined by the equivalent of Fresnel's formulas for elastic media.[9] The pressure ratio at the interface can be written in the following form:

$$\frac{\bar{p}}{p} = \frac{\bar{\rho}(\bar{c}_1{}^2 - 4\bar{c}_2{}^2/3)c_1{}^2}{\rho(c_1{}^2 - 4c_2{}^2/3)\bar{c}_1{}^2} \cdot \frac{3M\cos\zeta}{KM + LN} \tag{3}$$

where

$$K = \cos\zeta\left(\frac{\bar{\rho}}{\rho} + n\sin\zeta\right)\frac{c_1}{\bar{c}_1}\left[1 - \left(\frac{\bar{c}_1}{c_1}\sin\zeta\right)^2(1 - n\sin^2\zeta)\right]^{1/2}$$

$$M = \left(\frac{\bar{\rho}}{\rho} + n\sin^2\zeta\right)\frac{c_2}{\bar{c}_2}\left[\frac{1 - (\bar{c}_2/c_1)^2\sin^2\zeta}{1 - (c_2/c_1)^2\sin^2\zeta}(1 - n\sin^2\zeta)\right]^{1/2}$$

$$L = \frac{c_2}{c_1}\frac{\sin\zeta}{\left[1 - \left(\frac{c_2}{c_1}\sin\zeta\right)^2\right]^{1/2}}\left(1 = \frac{\bar{\rho}}{\rho} - n\sin^2\zeta\right) - \frac{c_1}{\bar{c}_1}n\sin\zeta\left[1 - \left(\frac{\bar{c}_1}{c_1}\sin\zeta\right)^2\right]^{1/2}$$

$$N = \left(1 - \frac{\bar{\rho}}{\rho} - n\sin^2\right)\sin\zeta - \frac{c_1}{\bar{c}_2}n\sin\zeta\cos\zeta \times \left[1 - \left(\frac{\bar{c}_2}{c_1}\sin\zeta\right)^2\right]^{1/2}$$

$$n = 2\left[\left(\frac{c_2}{c_1}\right)^2 - \frac{\bar{\rho}}{\rho}\left(\frac{\bar{c}_2}{c_1}\right)^2\right]$$

The quantities with a bar refer to the inclusion whereas the quantities without a bar refer to the matrix.

Let $\bar{p}_B$ and p_B be pressure at point B in Fig. 5 on the side of medium 2 and medium 1 respectively.

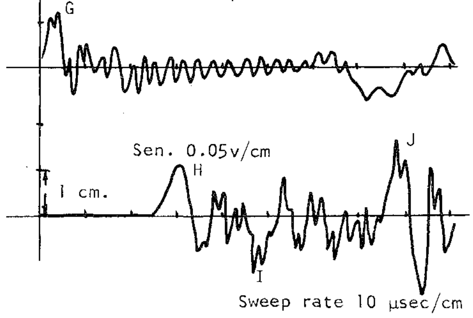

Fig. 8 Strain histories of an equivalent plate as the steel-aluminum specimen except without the steel inclusion.

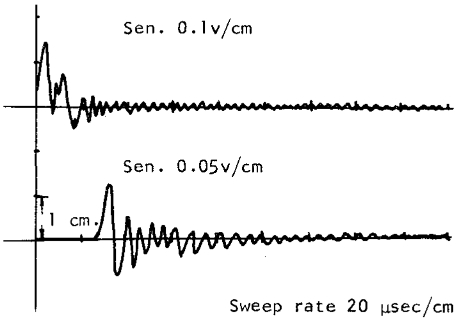

Fig. 9 Disappearance of peaks due to reflected waves in the strain histories of a large aluminum plate.

The pressure p_B can be determined by using Eq. (2)

$$p_B = p_0[b/L_{AB}]^{1/2}$$

where p_0 is the pressure at point 0 and b is the length of the straight ray AO; and the refracted pressure $\bar{p}_B$ can then be determined by using Eq. (3). Then, Eq. (2) is used to relate points B and C

$$\bar{p}_C/\bar{p}_B = [\bar{R}_B/\bar{R}_C]^{1/2}$$

where $\bar{R}_B$ is the radius of curvature of the wave fronts at point B in medium 2, and $\bar{R}_C$ is the radius of curvature of the wave front at point C in medium 2. The radius of curvature, $\bar{R}_B$, of the refracted wave fronts at point B can be obtained by considering two neighboring points on the interface, B and B′ as shown in Fig. 5. The angle of refraction at B′ is

$$\phi_{B'} \sim \phi + (d\phi/d\zeta)(\Delta\zeta + \Delta\theta)$$

From Snell's Law [Eq. (1)], we find $d\phi/d\zeta = \tan\phi/\tan\zeta$.

The following relations are deduced from Fig. 5:

$$\Delta\zeta = \mathrm{BN}/L_{AB}, \quad \Delta\theta = \overline{\mathrm{BB}'}/a,$$

and

$$(d\phi/d\zeta)(\Delta\zeta + \Delta\theta) - \Delta\theta = \overline{\mathrm{B'M}}/\bar{R}_B$$

Also $\mathrm{BN} = \overline{\mathrm{BB}'}\cos\zeta$, $\overline{\mathrm{B'M}} = \overline{\mathrm{BB}'}\cos\phi$. After substituting and simplifying, we obtain:

$$\bar{R}_B = \cos\phi\left[\frac{\tan\phi}{\tan\zeta}\left(\frac{\cos\zeta}{L_{AB}} + \frac{1}{a}\right) - \frac{1}{a}\right]^{-1}$$

Since the rays are straight lines normal to the wave front in both medium we obtain

$$\bar{R}_C = \bar{R}_B + L_{BC}$$

The pressure p_C can be determined from Eq. (3) where p_C is the pressure at point C after being refracted out of the inclusion to the matrix. Then using Eq. (2)

$$p_D/p_C = [R_C/R_D]^{1/2}$$

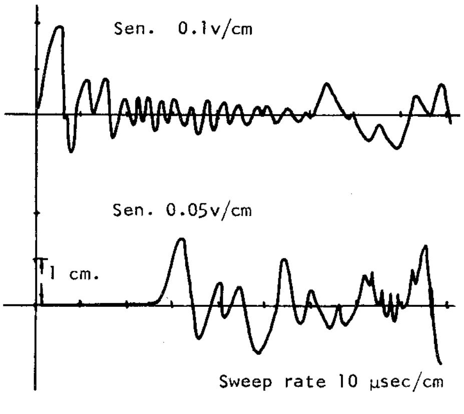

Fig. 10 Strain histories due to explosive loading on a single-inclusion steel-aluminum specimen, 5° ray.

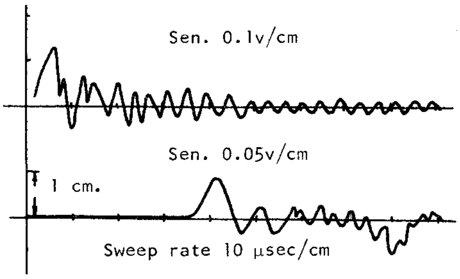

Fig. 11 Strain histories due to explosive loading on a single-inclusion steel-brass specimen, 0° ray.

The derivation of the radius of curvature R_C follows the same procedure as before:

$$R_C = \cos(\phi+\delta)\left[\frac{\tan(\phi+\delta)}{\tan\phi}\left(\frac{\cos\phi}{\bar{R}_C} - \frac{1}{a}\right) + \frac{1}{a}\right]^{-1}$$

Again, since the rays are straight lines normal to the wave front in each medium, $R_D = R_C + L_{CD}$.

Figure 6 shows an example of the pressure p as a function of position when the wave front arrives. The results are shown in the form of contour lines of constant pressure. The material constants used are $c_2/c_1 = 1.39$, and characteristic impedance ratio = 1.27. The pressure at point 0 is taken to be unity. Figure 6, when used in conjunction with Fig. 4, enables one to determine the pressure at the wave front for a given t. The wave fronts obtained in Fig. 4 are also shown in Fig. 6. Clearly, one can continue this procedure to determine the wave fronts and the pressure at the wave fronts for more than one inclusion.

Results

The magnitude and shape of the experimental strain histories were plotted from typical oscilloscope traces. A sample plot for the aluminum specimen with a single steel inclusion is shown in Fig. 7. The result was due to the detonation of a charge of lead azide at point A (see Fig. 1). The upper and lower traces correspond to the strain measured by the two pairs of strain gages which are located along the 0° ray, 4 in. and 10 in. from the point of detonation. The center of the 2-in.-diam inclusion is midway between the gages.

A rise time of 4 μsec was observed on both traces for the pressure pulse to reach its peaks G and H. The delay time of 29 μsec for the arrival of the pressure pulse between the gages correlated very well with the theoretically computed delay time of 29.5 μsec. The amplitude ratio of the peak strain, H/G, for the two strain gage measurements is 0.52. This compared very well with the amplitude ratio of 0.55 calculated from the ray theory. Another experiment was conducted on a specimen of the same dimension except without the inclusion. The result is shown in Fig. 8. The amplitude ratio of the peak strains, H/G, is 0.60

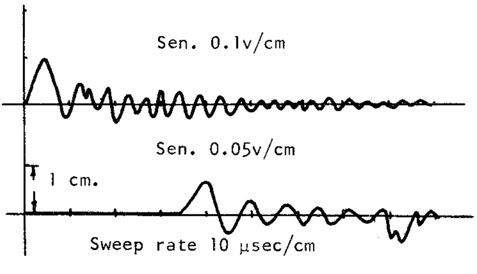

Fig. 12 Strain histories due to explosive loading on a single-inclusion steel-brass specimen, 4° ray.

Table 1 Summary of results

	Material	Location of strain gages, in.	Inclusions	Ray θ, deg.	Peak amplitude ratio, H/G	
					Experimental	Theoretical
I Explosive	Steel-aluminum	E = 4	1	0	0.52	0.55
		F = 10		5	0.46	0.52
	Steel-Brass	E = 3	1	0	0.45	0.43
		F = 9		4	0.47	0.42
		E = 1.8	2	0	0.29	0.315
		F = 9				
		E = 2.4	3	0	0.31	0.34
		F = 10				
		E = 2.4	4	0	0.50	0.56
		F = 10				
II Ram impingement	Steel-aluminum	E = 3	1	0	0.53	0.55
		F = 10				
	Steel-Brass	E = 3	1	0	0.42	0.43
		F = 9				
		E = 1.8	2	0	0.32	0.315
		F = 9				
		E = 2.4	3	0	0.34	0.34
		F = 10				
		E = 2.4	4	0	0.50	0.56
		F = 10				
III	Aluminum	E = 4	0		0.60	0.63
		F = 10				
		E = 3	0		...	0.57
		F = 9				
		E = 2.4	0		...	0.49
		F = 10				
		E = 1.8	0		...	0.445
		F = 9.0				

as compared with a theoretically calculated value of 0.63. The delay time between the two gages again correlated well with the theoretically computed delay time. It should be noted that the amplitude ratio of the peak strains has been attenuated from 0.60 to 0.50 for the plate with the inclusion.

The strain variation at the location of each gage is also analyzed as a function of time. However, the calculation gets very complicated with the existence of the reflected and refracted waves. When there exists a large number of interfaces as in the cases of specimens with multiple inclusions or specimens with small overall dimensions, the calculation becomes virtually impossible and some effective modulus theory must be used. The pulse reflection from the back free surface is also shown in Figs. 7 and 8 with the peak tensile amplitude I. The rather high peak amplitude J can be attributed to the multiple reflections along the 0° ray and to the reflections from the sides of the square plate which arrived at the second gage approximately, 90 μsec after the initial detonation of the charge. Both peaks, I and J appeared during tests on plates of the same dimension with or without the inclusion; and disappeared during tests on a similar plate but with a dimension of 48 in. × 48 in. as can be seen from Fig. 9.

Additional sample results are presented in Figs. 10–14. Figure 10 gives the strain histories of the same steel-aluminum specimen along a 5° ray. Figures 11 and 12 are the results for a steel-brass plate with one inclusion along rays $\theta = 0°$ and 4°. Figure 13 presents the strain histories for a steel-brass plate with two inclusions.

While the above are the results due to explosive loading, the strain histories of the steel-brass plate with a single inclusion

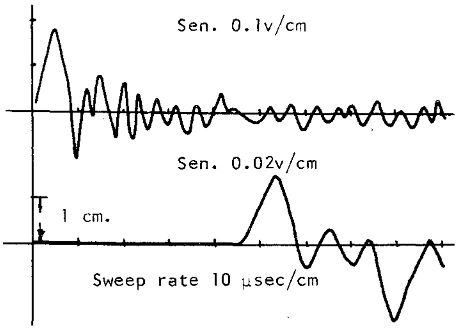

Fig. 13 Strain histories due to explosive loading on a two-inclusion steel-brass specimen, 0° ray.

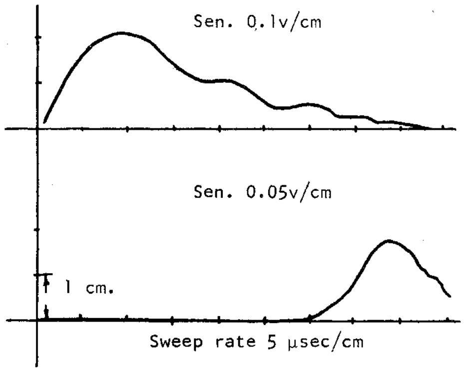

Fig. 14 Strain histories due to impingement loading on a single-inclusion steel-brass specimen, 0° ray.

due to impingement of the ram against the plate at A (see Fig. 1) are presented in Fig. 14. The risetime has a much larger value of 10 μsec compared to 4 μsec for the explosive loading.

Additional experiments using both methods were performed on plates with two, three, or four inclusions. The results of all the experiments are summarized in Table 1.

Table 1 is divided into three parts. Parts I and II refer to the two methods of pulse generation. Part III lists the theoretically computed peak ratios, H/G for several selected gage locations. The results are based on Eq. (2) and are for homogeneous material. The first four columns in Table 1 give, respectively, the composites tested, the location of the strain gages, the number of inclusions, and the identity of the rays. The last two columns give the average experimental results and the results obtained by the ray theory presented in this paper.

Conclusion

Experimental results on steel-aluminum and steel-brass inclusion-matrix composites using explosives and ram impingement compared very well with the analytically computed results using ray theory.

With good agreement between the experimental and theoretically computed results, one can confidently proceed in applying the theory to fiber-reinforced composites to determine the optimum micro-structural variables such as modulus of elasticity ratio (fiber to matrix), relative fiber size, and orientation to increase resistance to stress fracture.

References

[1] Thomas, T. Y., *Plastic Flow and Fracture in Solids,* Academic Press, New York, 1964.

[2] Luneburg, R. K., *Mathematical Theory of Optics,* University of California Press, Los Angeles, Calif., 1964.

[3] Friedlander, F. G., *Sound Pulses,* Cambridge University Press, Cambridge, Mass., 1958.

[4] Keller, H., "Propagation of Stress Discontinuities in Inhomogeneous Elastic Media," *SIAM Review,* Vol. 6, No. 4, Oct. 1964, pp. 356–382.

[5] Ting, T. C. T. and Lee, E. H., "Wave Front Analysis in Composite Materials," *Journal of Applied Mechanics,* Vol. 36, Sept. 1969, pp. 497–504.

[6] Achenbach, J. D., Hemann, J. H., and Ziegler, F., "Separation at the Interface of a Circular Inclusion and the Surrounding Medium Under an Incident Compressive Wave," *Journal of Applied Mechanics,* Vol. 37, Ser. E, June 1970, pp. 298–304.

[7] Nariboli, G. A., "Wave Propagation in Anisotropic Elasticity," *Journal of Mathematical Analysis and Applications,* Vol. 16, Oct. 1966, pp. 108–120.

[8] Ben-Amoz, M., "The Dynamic Behavior of Tape Wound Shields Under Normal-to-Surface Impact Loads," Rept. TM SM 8156-24, Feb. 1968, Reentry Systems Dept., General Electric Co., Pa.

[9] Ewing, W. M., Jardetzky, W. S., and Press, F., *Elastic Waves in Layered Media,* McGraw-Hill, New York, 1957, pp. 76–87.